EXTENDED METHODS

Plasmids

pBabe-puro-BRAF and pBabe-puro-BRAF^{V600E} were obtained from Dr. William Hahn (1). BRAF WT and V600E cDNAs were subcloned into pcDNA3-HA and pFlag-CMV vectors. HA-FZR1, HA-CDC20, Myc-FZR1 and GST-FZR1 were described previously (2). shRNA constructs targeting human FZR1 (RHS4533-EG51343), mouse FZR1 (RHS4534-EG56371), human CDC20 (RHS4533-EG991), mouse CDC20 (RHS4534-EG107995), human APC10 (RHS4533-EG10393), mouse APC10 (RHS4534-EG68999), human CDC27 (RHS4533-EG996), human BRAF (RHS4533-EG4157) and mouse BRAF (RMM4534-EG17199) were purchased from OpenBiosystems. FZR1 cDNA for rescue experiments were mutated to be resistant to shFZR1 depletion (3). Site directed mutagenesis to generate various BRAF D-box mutants was performed using the QuikChange XL Site-Directed Mutagenesis Kit (Stratagene) according to the manufacturer's instructions.

Antibodies

Anti-BRAF (9433), anti-CRAF (9422), anti-ARAF (4432), anti-PTEN (9188), anti-AURORA A (3092), anti-AKT (pan) (2920), anti-pS473-AKT (4070), anti-pT202/pY204-ERK1/2 (4370), anti-ERK1/2 (4695), anti-p-MAPK/CDK Substrates (PXS*P or S*PXR/K) (2325), anti-pS217/pS221-MEK1/2 (9154), anti-MEK1/2 (9122) antibodies were purchased from Cell Signaling Technology. Anti-CYCLIN A2 (H-432), anti-PLK1 (F-8), anti-APC10 (B-1), anti-CDC6 (180.2), anti-CDC27 (AF3.1), anti-CDC20 (E-7), anti-p16 (F-12), anti-p21 (C-19), anti-p-ELK-1 (B-4), anti-ELK-1 (3H6D12), anti-c-Myc (9E10) and polyclonal anti-HA (Y-11) antibodies were purchased from Santa Cruz. Anti-APC4 (A301-176A), anti-APC8 (A301-181A), anti-TUBULIN (T-5168) and anti-VINCULIN (V-4505) antibodies were purchased from Bethyl Labs. Polyclonal anti-Flag antibody (F-2425), monoclonal anti-Flag (F-3165) antibody, anti-Flag agarose beads (A-2220), anti-HA agarose beads (A-2095) as well as peroxidase-conjugated anti-mouse secondary antibody (A-4416) and peroxidase-conjugated anti-rabbit secondary antibody (A-4914) were purchased from Sigma. Monoclonal anti-HA antibody (MMS-101P) was purchased from Covance. Anti-GFP antibody (632380) and polyclonal anti-FZR1 antibody (34-2000) were purchased from Invitrogen. Monoclonal anti-FZR1 (CC43) was purchased from Calbiochem.

Justification of Different Cell Lines Used in This Study

Human primary melanocytes (HPM) and murine normal melanocytes melan-a are used mainly in Fig. 1 and Fig. 2 to demonstrate that in the normal melanocyte setting, depletion of *FZR1* leads to BRAF accumulation, ERK activation and subsequent senescence. HPM and melan-a are the most widely used *in vitro* melanocyte culture for melanogenesis studies (5, 6).

HeLa and HEK293 cell lines were used for ectopic expression-based degradation/ubiquitination assays mainly in Fig. 3 and Fig. 4, which are widely used in the ubiquitin and APC research fields (7, 8). In addition, HEK293 cells have also been widely used to study the MAPK signaling pathway (9, 10).

HEK293T cell line is used mainly in Fig. 3 and Fig. 4 for co-IP assays to define the interaction between two ectopically expressed proteins, which is the most frequently used cell line for this type of experiment.

HBL, U2OS, OVCAR8 and T98G cancer cell lines were mainly used in Fig. 4 and Fig. 5 as BRAF^{WT} expressing cell lines to analyze how FZR1 controls the BRAF/ERK signaling pathway via disruption of BRAF dimerization.

A375, SK-MEL-28 and WM266.4 are widely used melanoma cell lines expressing the BRAF^{V600E} oncogenic mutation. These cell lines were mainly used in Fig. 5 to demonstrate that FZR1 failed to suppress the function of BRAF^{V600E}, while BRAF^{V600E} could inhibit the APC^{FZR1} E3 ligase activity through *N*-terminal phosphorylation of FZR1.

Immortalized human primary melanocytes (human primary melanocytes immortalized by inducing expression of hTERT, p53DD and CDK4(R24C), termed IHPM for short) is a kind gift from Dr. Hans Widlund (11). IHPM cell line has been used as an *in vitro* melanomagenesis system allows for experimental

reconstitution of the melanoma development process *in vitro* after altering the expression of certain genes, therefore it is widely utilized in the melanoma research field (11-15). IHPM cell line was mainly used in Fig.7 and Fig. S7 to examine whether co-depletion of FZR1 and PTEN could transform otherwise TPA-dependent IHPM cells.

Cell Synchronization

Cell synchronization with nocodazole arrest and double thymidine treatment, have been described previously (16, 17).

FACS Analysis

Cells synchronized with serum starvation and release or nocodazole-arrest and release were collected at the indicated time points and stained with propidium iodide (Roche) according to the manufacturer's instructions. Stained cells were sorted with a Dako-Cytomation MoFlo sorter (Dako) at the Dana-Farber Cancer Institute FACS core facility.

SUPPLEMENTARY REFERENCES

1. Boehm JS, Zhao JJ, Yao J, Kim SY, Firestein R, Dunn IF, et al. Integrative genomic approaches identify IKBKE as a breast cancer oncogene. Cell. 2007;129:1065-79.
2. Wan L, Zou W, Gao D, Inuzuka H, Fukushima H, Berg AH, et al. Cdh1 regulates osteoblast function through an APC/C-independent modulation of Smurf1. Molecular cell. 2011;44:721-33.
3. Gao D, Inuzuka H, Tseng A, Chin RY, Toker A, Wei W. Phosphorylation by Akt1 promotes cytoplasmic localization of Skp2 and impairs APCCdh1-mediated Skp2 destruction. Nat Cell Biol. 2009;11:397-408.
4. Boehm JS, Hession MT, Bulmer SE, Hahn WC. Transformation of human and murine fibroblasts without viral oncoproteins. Molecular and cellular biology. 2005;25:6464-74.
5. Du J, Widlund HR, Horstmann MA, Ramaswamy S, Ross K, Huber WE, et al. Critical role of CDK2 for melanoma growth linked to its melanocyte-specific transcriptional regulation by MITF. Cancer cell. 2004;6:565-76.
6. Ryu B, Moriarty WF, Stine MJ, DeLuca A, Kim DS, Meeker AK, et al. Global analysis of BRAFV600E target genes in human melanocytes identifies matrix metalloproteinase-1 as a critical mediator of melanoma growth. The Journal of investigative dermatology. 2011;131:1579-83.
7. Stegmeier F, Rape M, Draviam VM, Nalepa G, Sowa ME, Ang XL, et al. Anaphase initiation is regulated by antagonistic ubiquitination and deubiquitination activities. Nature. 2007;446:876-81.
8. Amador V, Ge S, Santamaria PG, Guardavaccaro D, Pagano M. APC/C(Cdc20) controls the ubiquitin-mediated degradation of p21 in prometaphase. Molecular cell. 2007;27:462-73.
9. Chen SH, Zhang Y, Van Horn RD, Yin T, Buchanan S, Yadav V, et al. Oncogenic BRAF Deletions That Function as Homodimers and Are Sensitive to Inhibition by RAF Dimer Inhibitor LY3009120. Cancer discovery. 2016;6:300-15.
10. Weber CK, Slupsky JR, Kalmes HA, Rapp UR. Active Ras induces heterodimerization of cRaf and BRaf. Cancer research. 2001;61:3595-8.
11. Garraway LA, Widlund HR, Rubin MA, Getz G, Berger AJ, Ramaswamy S, et al. Integrative genomic analyses identify MITF as a lineage survival oncogene amplified in malignant melanoma. Nature. 2005;436:117-22.
12. Haq R, Shoag J, Andreu-Perez P, Yokoyama S, Edelman H, Rowe GC, et al. Oncogenic BRAF regulates oxidative metabolism via PGC1alpha and MITF. Cancer cell. 2013;23:302-15.
13. Jalili A, Wagner C, Pashenkov M, Pathria G, Mertz KD, Widlund HR, et al. Dual suppression of the cyclin-dependent kinase inhibitors CDKN2C and CDKN1A in human melanoma. Journal of the National Cancer Institute. 2012;104:1673-9.
14. Van Raamsdonk CD, Bezrookove V, Green G, Bauer J, Gaugler L, O'Brien JM, et al. Frequent somatic mutations of GNAQ in uveal melanoma and blue naevi. Nature. 2009;457:599-602.
15. Scott KL, Nogueira C, Heffernan TP, van Doorn R, Dhakal S, Hanna JA, et al. Proinvasion metastasis drivers in early-stage melanoma are oncogenes. Cancer cell. 2011;20:92-103.
16. Wan L, Tan M, Yang J, Inuzuka H, Dai X, Wu T, et al. APC(Cdc20) suppresses apoptosis through targeting Bim for ubiquitination and destruction. Developmental cell. 2014;29:377-91.
17. Wei W, Ayad NG, Wan Y, Zhang GJ, Kirschner MW, Kaelin WG, Jr. Degradation of the SCF component Skp2 in cell-cycle phase G1 by the anaphase-promoting complex. Nature. 2004;428:194-8.
18. Haqq C, Nosrati M, Sudilovsky D, Crothers J, Khodabakhsh D, Pulliam BL, et al. The gene expression signatures of melanoma progression. Proc Natl Acad Sci U S A. 2005;102:6092-7.
19. da Fonseca PC, Kong EH, Zhang Z, Schreiber A, Williams MA, Morris EP, et al. Structures of APC/C(Cdh1) with substrates identify Cdh1 and Apc10 as the D-box co-receptor. Nature. 2011;470:274-8.
20. Wan PT, Garnett MJ, Roe SM, Lee S, Niculescu-Duvaz D, Good VM, et al. Mechanism of activation of the RAF-ERK signaling pathway by oncogenic mutations of B-RAF. Cell. 2004;116:855-67.

21. He J, Chao WC, Zhang Z, Yang J, Cronin N, Barford D. Insights into degron recognition by APC/C coactivators from the structure of an Acm1-Cdh1 complex. Molecular cell. 2013;50:649-60.
22. Pettersen EF, Goddard TD, Huang CC, Couch GS, Greenblatt DM, Meng EC, et al. UCSF Chimera--a visualization system for exploratory research and analysis. J Comput Chem. 2004;25:1605-12.
23. Poulikakos PI, Rosen N. Mutant BRAF melanomas--dependence and resistance. Cancer cell. 2011;19:11-5.
24. Cerami E, Gao J, Dogrusoz U, Gross BE, Sumer SO, Aksoy BA, et al. The cBio cancer genomics portal: an open platform for exploring multidimensional cancer genomics data. Cancer discovery. 2012;2:401-4.
25. Gao J, Aksoy BA, Dogrusoz U, Dresdner G, Gross B, Sumer SO, et al. Integrative analysis of complex cancer genomics and clinical profiles using the cBioPortal. Science signaling. 2013;6:pl1.

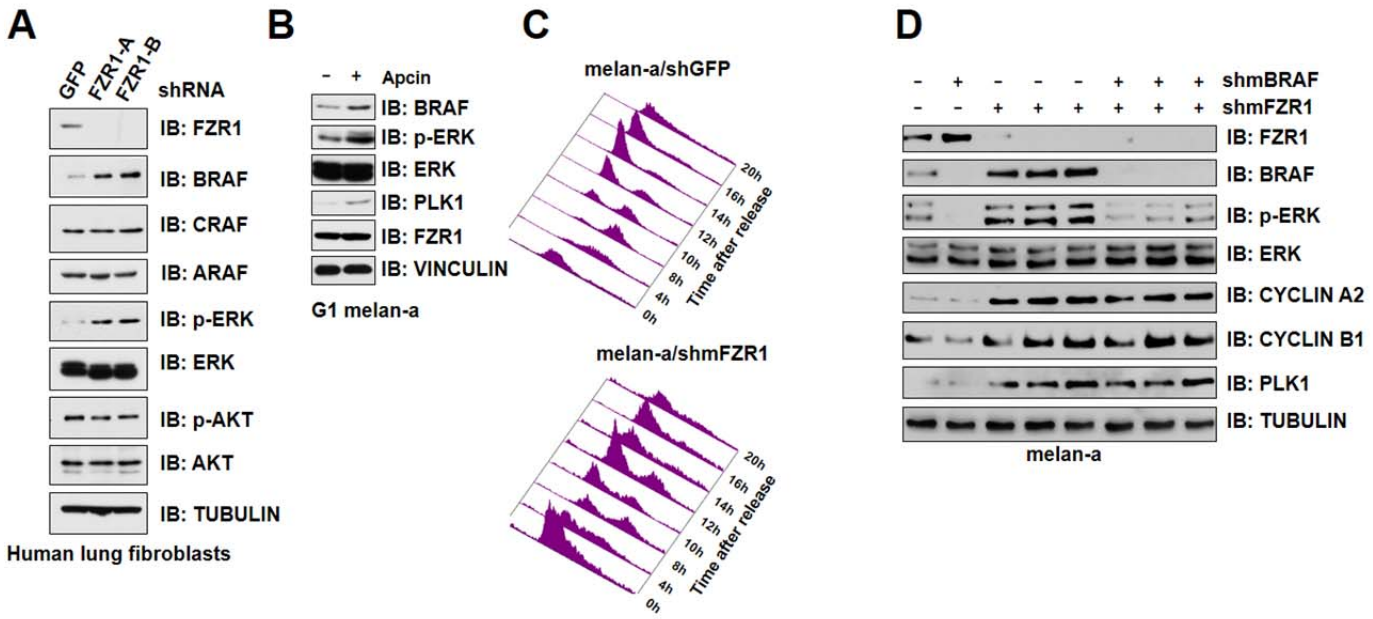

Figure S1. Depletion of *FZR1* leads to BRAF stabilization and subsequent ERK activation.

(A) Depletion of *FZR1* led to an elevation of BRAF and its downstream MEK/ERK activities in human lung fibroblasts. Immunoblot (IB) analysis of human lung fibroblasts infected with control (shGFP) or sh*FZR1* lentiviral shRNA constructs. The infected cells were selected with 1 μg/ml puromycin for 72 hours before harvesting.

(B) Inhibition of APC^{FZR1} by Apcin led to BRAF upregulation in G1 phase melan-a cells. melan-a cells were synchronized at G1 as described in Fig. **1C** and the cells were treated with 25 μM Apcin for 2 hours before harvesting.

(C) FACS analysis was performed to monitor cell cycle changes for melan-a cells in Fig. **1C.**

(D) Additional depletion of *BRAF* suppressed the activation of ERK upon *FZR1* knockdown. IB analysis of melan-a infected with the indicated lentiviral shRNA constructs. The infected cells were selected with 1 μg/ml puromycin for 72 hours to eliminate the non-infected cells before harvesting.

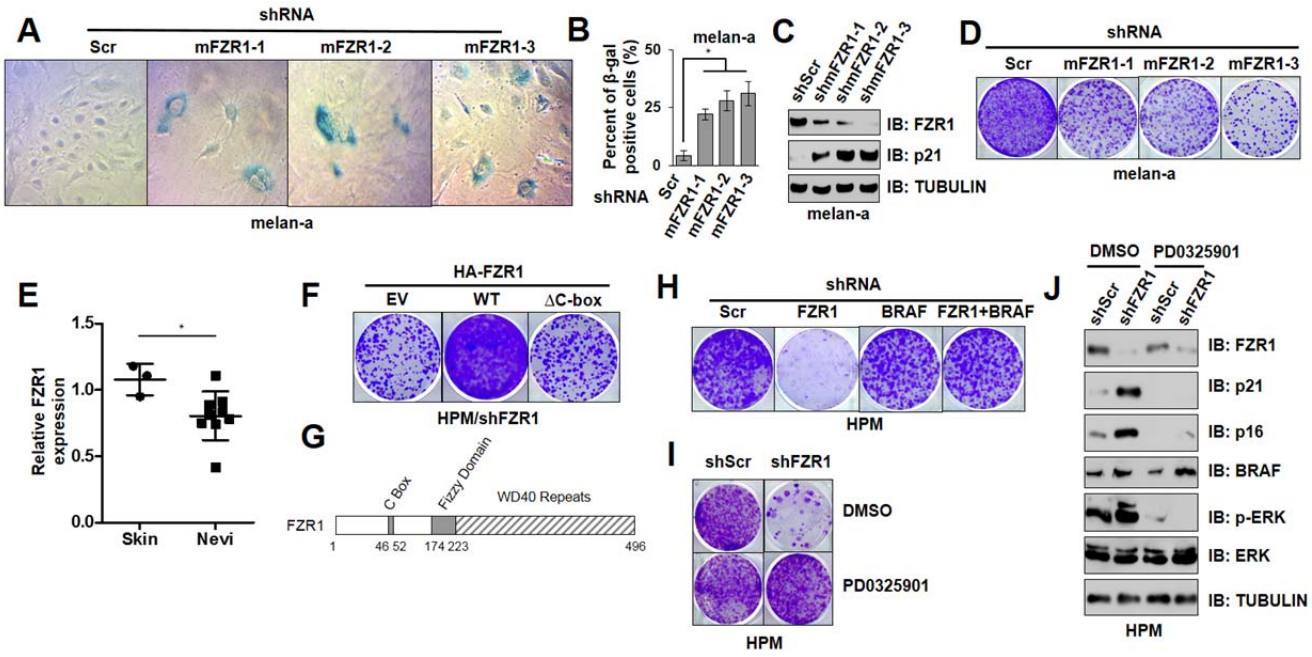

Figure S2. Depletion of *FZR1* triggers the onset of premature senescence in primary melanocytes.

(A-B) Depletion of *FZR1* in melan-a cells triggered premature senescence. shScr or sh*FZR1* infected mouse melanocytes (melan-a) were subjected to SA-β-gal staining assays 14 days after viral infection. The pictures showed one representative experiment (**A**) out of three independent experiments. Data are represented as mean ± SD, n=3. * $p < 0.05$, Student's *t* test (**B**).

(C) *FZR1* knockdown resulted in the accumulation of CDK inhibitor p21 in melan-a cells. Immunoblot (IB) analysis of melan-a cells generated in (**A**).

(D) Depletion of *FZR1* retarded the proliferation of melan-a cells. Control (shScr) or sh*FZR1* infected melan-a cells were subjected to clonogenic survival assays 5 days after viral infection. Crystal violet was used to stain the formed colonies.

(E) *FZR1* expression is significantly reduced in clinical *nevi* samples (n=9) compared with normal skin samples (n=3), the dataset was reported in (18), * $p < 0.05$, Student's *t* test.

(F) Ectopic re-introduction of WT-FZR1, but not APC-binding deficient ΔC-box-FZR1, rescued the retarded proliferation of *FZR1*-depleted HPMs. Control (shScr) or sh*FZR1* infected HPMs cells were subjected to clonogenic survival assays 5 days after viral infection. Crystal violet was used to stain the formed colonies.

(G) A schematic illustration of the domain structure of FZR1 with highlighted C-box-motif and Fizzy domain, both of which are critical for FZR1 association with the APC core complex.

(H) Control (shScr), sh*FZR1*, sh*BRAF* and sh*FZR1*+sh*BRAF* infected HPMs were subjected to clonogenic survival assays 5 days after the viral infection. Crystal violet was used to stain formed colonies.

(I) MEK inhibition reversed the suppressed proliferation of *FZR1*-depleted melanocytes. Control (shScr) or sh*FZR1* infected HPMs were treated with or without 1 μM MEK inhibitor PD0325901 and subjected to clonogenic survival assays 5 days after the viral infection. Crystal violet was used to stain the formed colonies.

(J) MEK inhibition blocked the upregulation of CDK inhibitors upon *FZR1* knockdown. IB analysis of melan-a cells generated in (**I**).

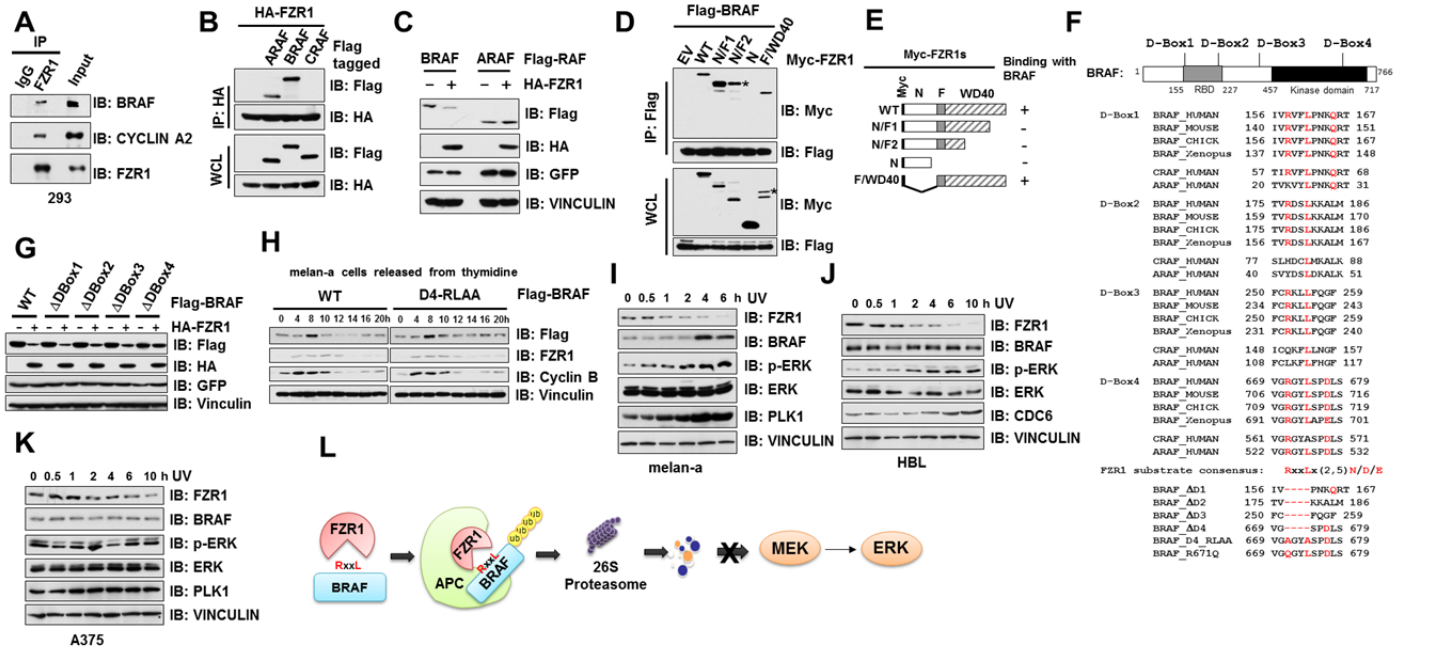

Figure S3. APC^{FZR1} promotes BRAF ubiquitination and subsequent degradation in a D-box dependent manner.

(A) Endogenous BRAF bound to endogenous FZR1 in cells. Immunoblot (IB) analysis of whole cell lysates (WCL) and anti-FZR1 immunoprecipitates (IP) derived from HEK293 cells.

(B) FZR1 specifically bound to ARAF and BRAF, but not CRAF, in cells. IB analysis of WCL and anti-HA IP derived from HEK293 cells transfected with HA-FZR1 and the indicated Flag-RAF constructs. 36 hours post-transfection, cells were pretreated with 10 μM MG132 for 10 hours before harvesting.

(C) FZR1 promoted the degradation of BRAF, but not ARAF in cells. IB analysis of WCL derived from HEK293 cells transfected with either Flag-BRAF or Flag-ARAF and HA-FZR1 where indicated. GFP serves as an internal transfection control.

(D) BRAF interacted with FZR1 primarily via its WD40 repeats domain, where it binds to substrates. IB analysis of WCL and IP derived from 293T cells transfected with Flag-BRAF and the indicated Myc-tagged FZR1 constructs. 36 hours post-transfection, cells were pretreated with 10 μM MG132 for 10 hours before harvesting. Asterisks (*) indicate non-specific bands.

(E) A schematic illustration to demonstrate that BRAF mainly interacts with the WD40 domain, but not the N terminal domain of FZR1.

(F) Sequence alignments of the four putative D-boxes containing region among BRAF proteins from various species as well as a schematic representation of the various D-box deletion or point mutation mutants generated and used in the following studies.

(G) Deletion of the D-box4 motif of BRAF largely attenuated FZR1-mediated BRAF degradation in cells. IB analysis of WCL derived from HEK293 cells transfected with the indicated Flag-BRAF individual D-box deletion mutants in the presence or absence of HA-FZR1. GFP serves as an internal transfection control.

(H) D4-RLAA-BRAF protein levels failed to fluctuate across the cell cycle. IB analysis of WCL derived from melan-a cells ectopically expressing WT- or D4-RLAA-BRAF synchronized at the G1/S boundary by double-thymidine block then released back into the cell cycle for the indicated periods of time.

(I-K) IB analysis of WCL derived from melan-a (**I**), HBL (**J**) or A375 (**K**) cells treated with 60 J/m^2 UV and cultured for the indicated time periods.

(L) A schematic illustration of the proposed models for APC^{FZR1}-mediated ubiquitination of BRAF in a D-box dependent manner.

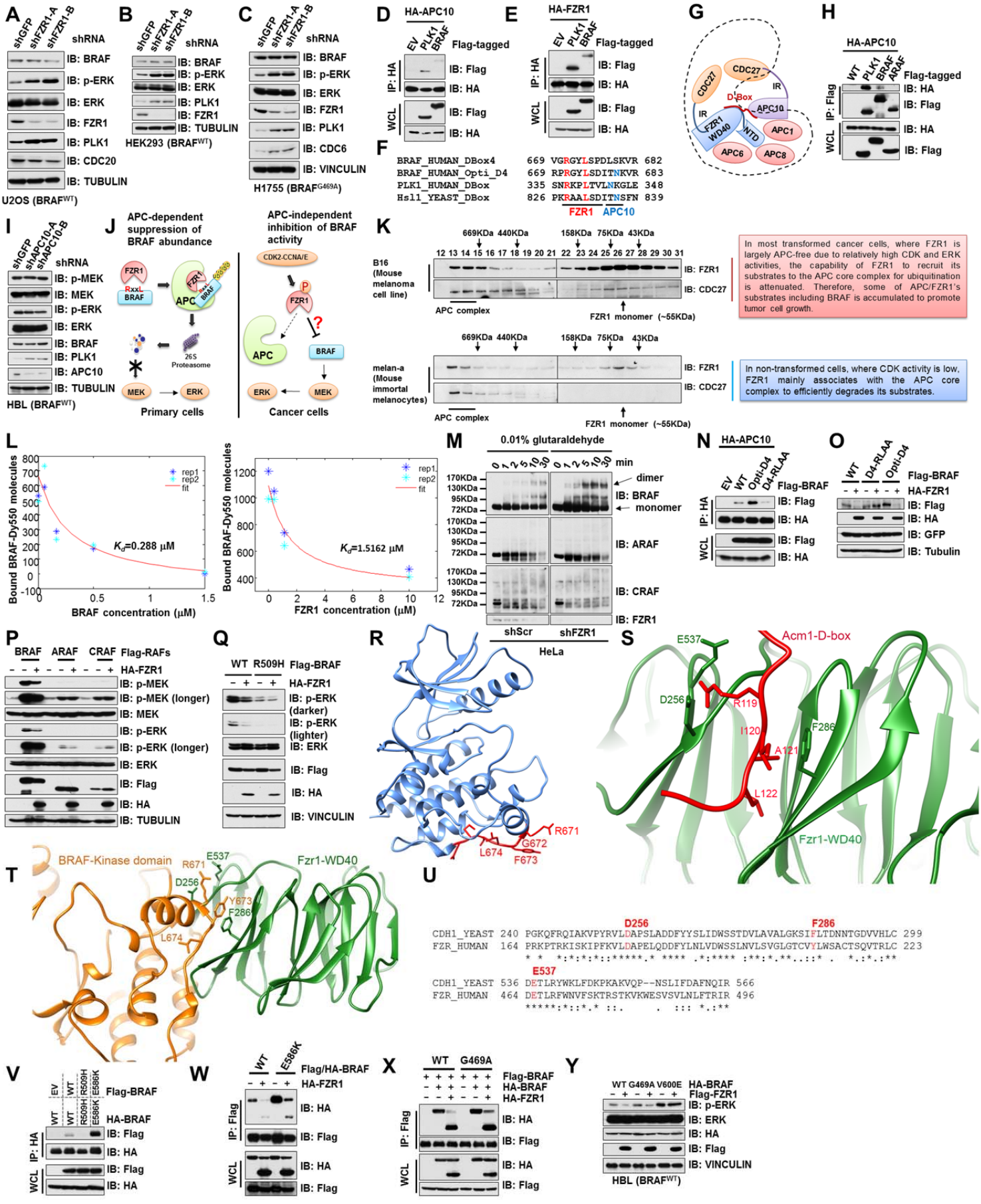
A
shGFP
shFZR1-A
shFZR1-B
shRNA
IB: BRAF
IB: p-ERK
IB: ERK
IB: FZR1
IB: PLK1
IB: CDC20
IB: TUBULIN
U2OS (BRAFWT)
B
shRNA
IB: BRAF
IB: p-ERK
IB: ERK
IB: PLK1
IB: FZR1
IB: TUBULIN
HEK293 (BRAFWT)
C
shRNA
IB: BRAF
IB: p-ERK
IB: ERK
IB: FZR1
IB: PLK1
IB: CDC6
IB: VINCULIN
H1755 (BRAFG469A)
D
HA-APC10
EV
PLK1
BRAF
Flag-tagged
IP: HA
IB: Flag
IB: HA
WCL
IB: Flag
IB: HA
E
HA-FZR1
EV
PLK1
BRAF
Flag-tagged
IP: HA
IB: Flag
IB: HA
WCL
IB: Flag
IB: HA
F
BRAF_HUMAN_DBox4 669 VGRGYLSPDLSKVR 682
BRAF_HUMAN_Opti_D4 669 RPRGYLSDITNKVR 683
PLK1_HUMAN_DBox 335 SNRKPLTVLNKGLE 348
Hsl1_YEAST_DBox 826 PKRAALSDITNSFN 839
FZR1
APC10
G
CDC27
CDC27
IR
D-Box
APC10
IR
FZR1
WD40
WTD
APC1
APC6
APC8
H
HA-APC10
WT
PLK1
BRAF
ARAF
Flag-tagged
IP: Flag
IB: HA
IB: Flag
WCL
IB: HA
IB: Flag
I
shGFP
shAPC10-A
shAPC10-B
shRNA
IB: p-MEK
IB: MEK
IB: p-ERK
IB: ERK
IB: BRAF
IB: PLK1
IB: APC10
IB: TUBULIN
HBL (BRAFWT)
J
APC-dependent suppression of BRAF abundance
FZR1
RxxL
BRAF
APC
FZR1
RxxL
BRAF
26S Proteasome
MEK
ERK
Primary cells
APC-independent inhibition of BRAF activity
CDK2-CCNA/E
P
FZR1
?
APC
BRAF
ERK
MEK
Cancer cells
K
669KDa 440KDa
158KDa 75KDa 43KDa
12 13 14 15 16 17 18 19 20 21 22 23 24 25 26 27 28 29 30 31
B16 (Mouse melanoma cell line)
IB: FZR1
IB: CDC27
APC complex
FZR1 monomer (~55KDa)
In most transformed cancer cells, where FZR1 is largely APC-free due to relatively high CDK and ERK activities, the capability of FZR1 to recruit its substrates to the APC core complex for ubiquitination is attenuated. Therefore, some of APC/FZR1's substrates including BRAF is accumulated to promote tumor cell growth.
669KDa 440KDa
158KDa 75KDa 43KDa
melan-a (Mouse immortal melanocytes)
IB: FZR1
IB: CDC27
APC complex
FZR1 monomer (~55KDa)
In non-transformed cells, where CDK activity is low, FZR1 mainly associates with the APC core complex to efficiently degrades its substrates.
L
Bound BRAF-Dy550 molecules
rep1
rep2
fit
Kd=0.288 μM
BRAF concentration (μM)
Bound BRAF-Dy550 molecules
rep1
rep2
fit
Kd=1.5162 μM
FZR1 concentration (μM)
M
0.01% glutaraldehyde
0 1 2 5 10 30 0 1 2 5 10 30 min
170KDa
130KDa
95KDa
72KDa
dimer
IB: BRAF
monomer
IB: ARAF
IB: CRAF
IB: FZR1
shScr
shFZR1
HeLa
N
HA-APC10
EV
WT
Opti-D4
D4-RLAA
Flag-BRAF
IP: HA
IB: Flag
IB: HA
WCL
IB: Flag
IB: HA
O
WT
D4-RLAA
Opti-D4
Flag-BRAF
HA-FZR1
IB: Flag
IB: HA
IB: GFP
IB: Tubulin
P
BRAF
ARAF
CRAF
Flag-RAFs
HA-FZR1
IB: p-MEK
IB: p-MEK (longer)
IB: MEK
IB: p-ERK
IB: p-ERK (longer)
IB: ERK
IB: Flag
IB: HA
IB: TUBULIN
Q
WT
R509H
Flag-BRAF
HA-FZR1
IB: p-ERK (darker)
IB: p-ERK (lighter)
IB: ERK
IB: Flag
IB: HA
IB: VINCULIN
R
R671
L674
G672
F673
S
E537
Acm1-D-box
D256
R119
I120
F286
A121
L122
Fzr1-WD40
T
BRAF-Kinase domain
R671
E537
Fzr1-WD40
D256
Y673
F286
L674
U
D256
F286
CDH1_YEAST 240 PGKQFRQIAKVPYRVLDAPSLADDFYYSLIDWSSTDVLAVALGKSIFLTDNNTGDVVHLC 299
FZR_HUMAN 164 PRKPTRKISKIPFKVLDAPELQDDFYLNLVDWSSLNVLSVGLGTCVYLWSACTSQVTRLC 223
E537
CDH1_YEAST 536 DETLRYWKLFDKPKAKVQP--NSLIFDAFNQIR 566
FZR_HUMAN 464 DETLRFWNVFSKTRSTKVKWESVSVLNLFTRIR 496
V
EV
WT
R509H
E586K
Flag-BRAF
HA-BRAF
IP: HA
IB: Flag
IB: HA
WCL
IB: Flag
IB: HA
W
WT
E586K
Flag/HA-BRAF
HA-FZR1
IP: Flag
IB: HA
IB: Flag
WCL
IB: HA
IB: Flag
X
WT
G469A
Flag-BRAF
HA-BRAF
HA-FZR1
IP: Flag
IB: HA
IB: Flag
WCL
IB: HA
IB: Flag
Y
WT G469A V600E
HA-BRAF
Flag-FZR1
IB: p-ERK
IB: ERK
IB: HA
IB: Flag
IB: VINCULIN
HBL (BRAFWT)

Figure S4. FZR1 disrupts the BRAF dimerization process.

(A-C) Depletion of *FZR1* in various cancer cells led to ERK activation but not BRAF accumulation Immunoblot (IB) analysis of whole cell lysates (WCL) derived from WT-BRAF expressing U2OS (**A**), HEK293 (**B**) or G469A-BRAF expressing H1755 (**C**) cells, all of which express WT-BRAF, infected with control (shScr) or sh*FZR1* lentiviral shRNA constructs. The infected cells were selected with 1 μg/ml puromycin for 72 hours before harvesting.

(D) Compared to the optimal APC^{FZR1} substrate PLK1, the binding between BRAF and FZR1 was relatively weaker. IB analysis of WCL and IP derived from HEK293 cells transfected with HA-FZR1 and Flag-PLK1 or Flag-BRAF. 36 hours post-transfection, cells were pretreated with 10 μM MG132 for 10 hours before harvesting.

(E) Compared to the optimal APC^{FZR1} substrate PLK1, the binding between BRAF and APC10 was relatively weak. IB analysis of WCL and IP derived from HEK293 cells transfected with HA-APC10 and Flag-PLK1 or Flag-BRAF. 36 hours post-transfection, cells were pretreated with 10 μM MG132 for 10 hours before harvesting.

(F) A sequence alignment indicating that compared to various well-characterized APC^{FZR1} substrates, BRAF lacks the interacting motif for APC10, a co-receptor for efficient recognition of the canonical D-box motif (19).

(G) A schematic illustration of the reported structural model for recognition of D-box within a substrate by FZR1 and APC10 as D-box co-receptors (19).

(H) Compared to the optimal APC^{FZR1} substrate PLK1, BRAF only moderately bound to the D-box co-receptor APC10, while ARAF failed to bind APC10. IB analysis of WCL and IP derived from HEK293 cells transfected with HA-APC10 and the indicated Flag-RAF constructs. 36 hours post-transfection, cells were pretreated with 10 μM MG132 for 10 hours before harvesting.

(I) Depletion of APC core subunit *APC10* in HBL cells did not lead to ERK activation or BRAF accumulation. IB analysis of WCL derived from WT-BRAF expressing HBL cells infected with control (sh*GFP*) or the indicated sh*APC10* lentiviral shRNA constructs. The infected cells were selected with 1 μg/ml puromycin for 72 hours before harvesting.

(J) A schematic illustration of proposed models for APC-dependent function of FZR1 in suppressing BRAF abundance in primary cells where most FZR1 associates with the APC core complex, as well as an APC-independent function of FZR1 in controlling BRAF kinase activity in most cancer cells, where the majority of FZR1 resides in an APC-free mode due to elevated phosphorylation of FZR1 by CDK kinases.

(K) Gel filtration experiments to illustrate that FZR1 primarily associates with the APC core complex in un-transformed, primary cells with relatively lower CDK and ERK activities, while mainly exists as monomers in transformed melanoma cells with elevated CDK and ERK activities. IB analysis of the indicated fractionations derived from the gel filtration experiments using transformed B16 mouse melanoma cells (upper) or mouse primary melanocytes derived melan-a cells (lower) whole cell lysates (WCL). Prior to running cell lysates, the molecular weight resolution of the column was first estimated by running native molecular weight markers (Thyroglobulin ~669KD, Ferritin ~440KD, Aldolase ~158KD, Conalbumin ~75KD and Ovalbumin ~43KD) and determining their retention times on coomassie-stained SDS-PAGE protein gels.

(L) Titration curve of BRAF-BRAF interaction with unlabeled BRAF (left panel) or FZR1 (right panel) as a competitor, using the single molecule assay. Various concentrations of BRAF (left panel) or FZR1 (right panel) was mixed with 10 nM Dylight550-labeled BRAF, and tested in a single molecule assay for transient protein-protein interactions. Binding constant of BRAF dimerization (left panel) or between immobilized BRAF and FZR1 (right panel) was extracted by fitting the titration curve. Two experimental replicates were shown.

(M) IB analysis of WCL derived from shScr- and shFZR1-HeLa cells that were harvested in 0.5% NP40-containing PBS buffer following by treatment with 0.01% glutaraldehyde as a crosslinking agent for the indicated time periods.

(N) IB analysis of WCL and IP derived from 293 cells transfected with HA-APC10 and the indicated Flag-BRAF constructs. 36 hours post-transfection, cells were pretreated with 10 μM MG132 for 10 hours before harvesting.

(O) IB analysis of WCL derived from 293 cells transfected with HA-FZR1 and the indicated Flag-BRAF constructs.

(P) Ectopic expression of FZR1 only suppressed BRAF-mediated, but not ARAF or CRAF-mediated, MEK/ERK activation. IB analysis of WCL derived from HEK293 cells transfected with HA-FZR1 and the indicated Flag-RAF constructs.

(Q) Ectopic expression of FZR1 only suppressed WT-BRAF-mediated, but not dimerization-deficient R509H-BRAF-mediated, MEK/ERK activation. IB analysis of WCL derived from HEK293 cells transfected with the indicated Flag-BRAF constructs in the presence or absence of HA-FZR1.

(R) A structural illustration of the putative spatial location of the D-box4 motif (marked in red) in a reported BRAF crystal structure (20) (PDB ID: 1UWH).

(S) A structural illustration of the yeast Fzr1-WD40 domain in complex with the Acm1 D-box motif (21) (PDB ID: 4BH6).

(T) A structural modeling illustration of docking the BRAF kinase domain to the yeast Fzr1-WD40 domain. The structure model was generated using UCSF Chimera (22).

(U) A sequence alignment showing that the WD40 repeats domain sequence is highly conserved between human FZR1 and yeast Fzr1.

(V) IB analysis of WCL and IP derived from 293T cells transfected with Flag- and HA-tagged-$BRAF^{WT}$, the $BRAF^{R509H}$ dimerization-deficient or the $BRAF^{pE586K}$ constitutive dimerization constructs as indicated. 36 hours post-transfection, cells were pretreated with 10 μM MG132 for 10 hours before harvesting.

(W) IB analysis of WCL and IP derived from 293T cells transfected with Flag- and HA-tagged-$BRAF^{WT}$ or $BRAF^{E586K}$ constructs in the presence or absence of HA-FZR1 as indicated. 36 hours post-transfection, cells were pretreated with 10 μM MG132 for 10 hours before harvesting.

(X) FZR1 disrupted dimerization of both WT-BRAF and $BRAF^{G469A}$ in cells. IB analysis of WCL and immunoprecipitates (IP) derived from 293T cells transfected with Flag- and HA-tagged-$BRAF^{WT}$ or $BRAF^{G469A}$ constructs in the presence or absence of HA-FZR1 as indicated. 36 hours post-transfection, cells were pretreated with 10 μM MG132 for 10 hours before harvesting.

(Y) IB analysis of WCL derived from HBL cells transfected with the indicated HA-BRAF constructs in the presence or absence of Flag-FZR1 where indicated.

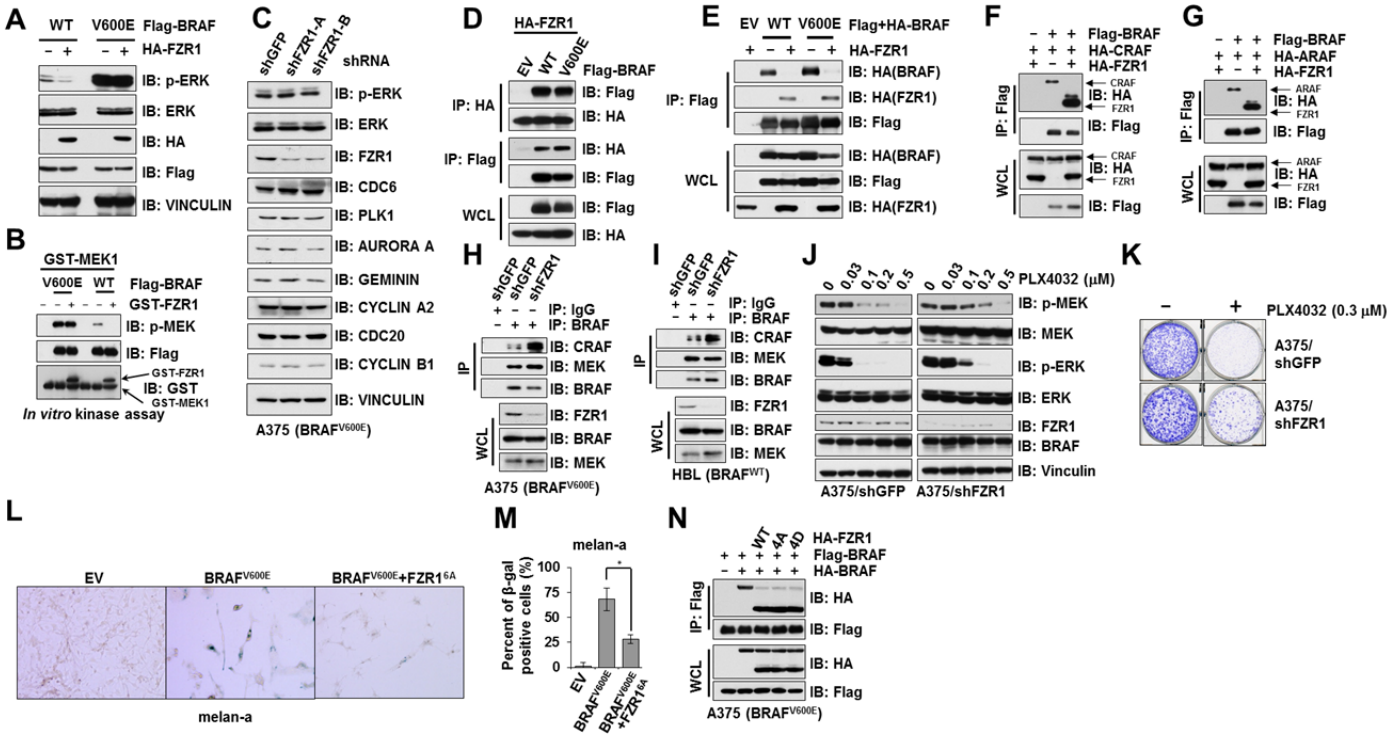

Figure S5. Phosphorylation of FZR1 N-terminus by ERK and CYCLIN D1/CDK4 inhibits the APC^{FZR1} E3 ubiquitin ligase activity.

(A) Unlike WT-BRAF, ERK activity mediated by BRAF^{V600E} was not affected by FZR1. Immunoblot (IB) analysis of whole cell lysates (WCL) derived from HEK293 cells transfected with the indicated Flag-BRAF constructs in the presence or absence of HA-FZR1 where indicated.

(B) *In vitro* kinase assays showing that FZR1 failed to inhibit the kinase activity of BRAF^{V600E}, which, unlike BRAF-WT kinase, is constitutively active regardless of its dimerization status (23).

(C) ERK activity was not affected upon depletion of *FZR1* in BRAF^{V600E}-expressing melanoma cells. IB analysis of BRAF^{V600E}-expressing A375 cells infected with control (shGFP) or sh*FZR1* lentiviral shRNA constructs. The infected cells were selected with 1 μg/ml puromycin for 72 hours before harvesting.

(D) FZR1 bound to both WT-BRAF and BRAF^{V600E} in cells. IB analysis of WCL and IP derived from 293T cells transfected with HA-FZR1 together with Flag-BRAF^{WT} or Flag-BRAF^{V600E}. 36 hours post-transfection, cells were pretreated with 10 μM MG132 for 10 hours before harvesting.

(E) FZR1 disrupted dimerization of both WT-BRAF and BRAF^{V600E} in cells. IB analysis of WCL and IP derived from 293T cells transfected with Flag- and HA-tagged-BRAF^{WT} or BRAF^{V600E} constructs in the presence or absence of HA-FZR1 as indicated. 36 hours post-transfection, cells were pretreated with 10 μM MG132 for 10 hours before harvesting.

(F) IB analysis of WCL and IP derived from 293T cells transfected with HA-FZR1 and Flag-BRAF or Flag-CRAF as indicated. 36 hours post-transfection, cells were pretreated with 10 μM MG132 for 10 hours before harvesting.

(G) IB analysis of WCL and IP derived from 293T cells transfected with HA-FZR1 and Flag-BRAF or Flag-ARAF as indicated. 36 hours post-transfection, cells were pretreated with 10 μM MG132 for 10 hours before harvesting.

(H-I) IB analysis of WCL and anti-BRAF IP derived from BRAF^{V600E}-expressing A375 (**H**) or BRAF^{WT}-expressing HBL (**I**) cells, infected with the control (shGFP) or shFZR1 lentiviral shRNA constructs. The infected cells were selected with 1 μg/ml puromycin for 72 hours to eliminate the non-infected cells before harvesting.

(J) shGFP- and shFZR1 infected $BRAF^{V600E}$-expressing A375 cells were treated with the indicated concentration of PLX4032 for 1 h before harvesting for IB analysis.

(K) $BRAF^{V600E}$-expressing A375 cells generated in (**J**) were subjected to clonogenic survival assays 5 days after viral infection. Crystal violet was used to stain the formed colonies and the colony numbers were counted.

(L-M) Expression of 6A-FZR1 led to partial resistance to $BRAF^{V600E}$-induced premature senescence in melan-a cells. pBabe-EV, $BRAF^{V600E}$ or $BRAF^{V600E}$+pLenti-6AFZR1 infected melan-a cells were subjected to SA-β-gal staining assays 14 days after viral infection. The pictures showed one representative experiment (**L**) out of three independent experiments. Data are represented as mean ± SD, n=3. * $p < 0.05$, Student's *t* test (**M**).

(N) IB analysis of WCL and IP derived from A375 cells transfected with HA-BRAF and Flag-BRAF, as well as the indicated HA-FZR1 constructs. 36 hours post-transfection, cells were pretreated with 10 μM MG132 for 10 hours before harvesting.

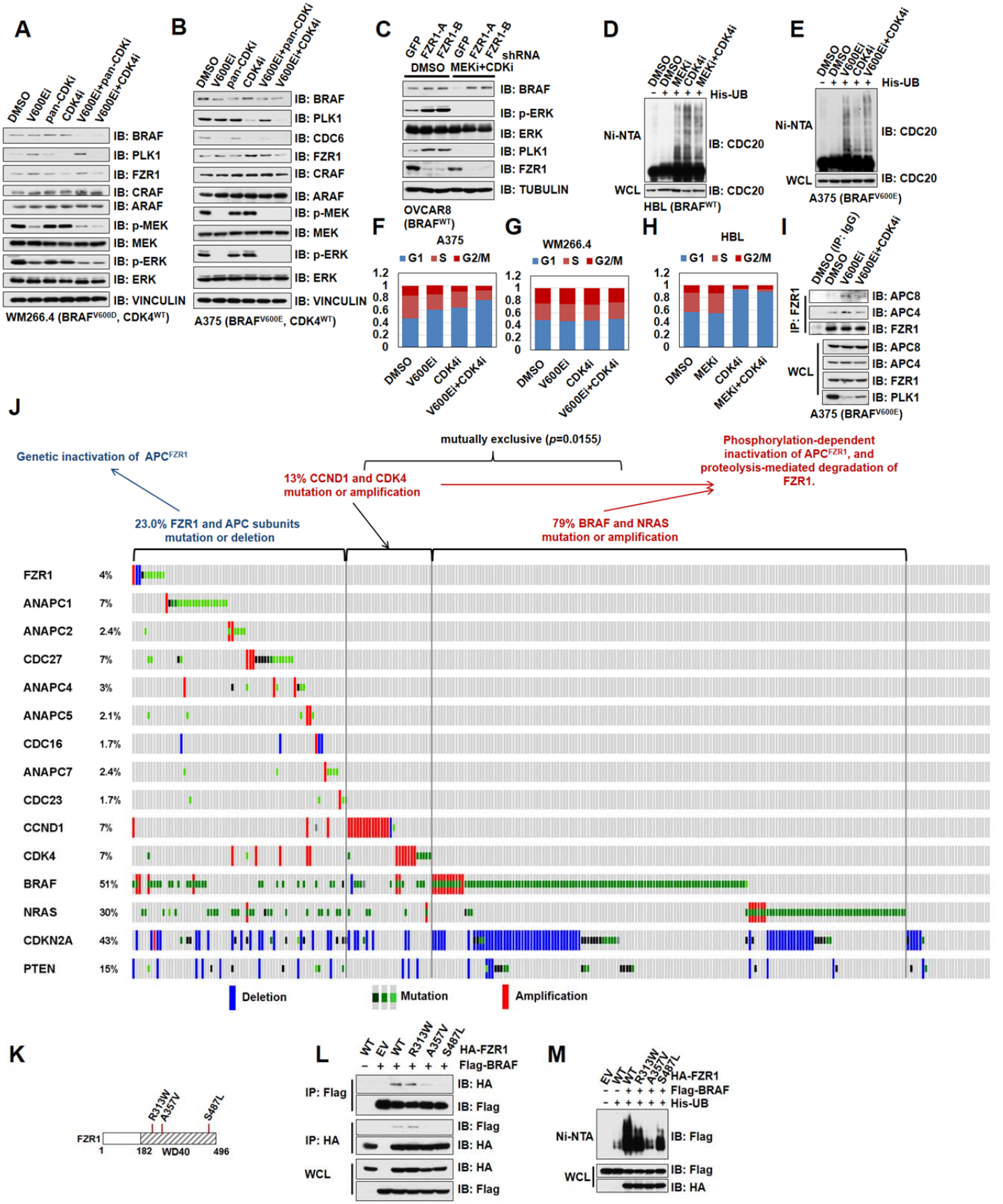
A
DMSO
V600Ei
pan-CDKi
CDK4i
V600Ei+pan-CDKi
V600Ei+CDK4i
IB: BRAF
IB: PLK1
IB: FZR1
IB: CRAF
IB: ARAF
IB: p-MEK
IB: MEK
IB: p-ERK
IB: ERK
IB: VINCULIN
WM266.4 (BRAFV600D, CDK4WT)
B
DMSO
V600Ei
pan-CDKi
CDK4i
V600Ei+pan-CDKi
V600Ei+CDK4i
IB: BRAF
IB: PLK1
IB: CDC6
IB: FZR1
IB: CRAF
IB: ARAF
IB: p-MEK
IB: MEK
IB: p-ERK
IB: ERK
IB: VINCULIN
A375 (BRAFV600E, CDK4WT)
C
GFP
FZR1-A
FZR1-B
shRNA
DMSO
MEKi+CDKi
IB: BRAF
IB: p-ERK
IB: ERK
IB: PLK1
IB: FZR1
IB: TUBULIN
OVCAR8 (BRAFWT)
D
DMSO
MEKi
CDK4i
MEKi+CDK4i
His-UB
Ni-NTA
IB: CDC20
WCL
IB: CDC20
HBL (BRAFWT)
E
DMSO
V600Ei
CDK4i
V600Ei+CDK4i
His-UB
Ni-NTA
IB: CDC20
WCL
IB: CDC20
A375 (BRAFV600E)
F
A375
G1
S
G2/M
DMSO
V600Ei
CDK4i
V600Ei+CDK4i
G
WM266.4
H
HBL
MEKi
I
DMSO (IP: IgG)
IP: FZR1
IB: APC8
IB: APC4
IB: FZR1
WCL
IB: PLK1
J
Genetic inactivation of APCFZR1
mutually exclusive (p=0.0155)
13% CCND1 and CDK4 mutation or amplification
Phosphorylation-dependent inactivation of APCFZR1, and proteolysis-mediated degradation of FZR1.
23.0% FZR1 and APC subunits mutation or deletion
79% BRAF and NRAS mutation or amplification
FZR1 4%
ANAPC1 7%
ANAPC2 2.4%
CDC27 7%
ANAPC4 3%
ANAPC5 2.1%
CDC16 1.7%
ANAPC7 2.4%
CDC23 1.7%
CCND1 7%
CDK4 7%
BRAF 51%
NRAS 30%
CDKN2A 43%
PTEN 15%
Deletion
Mutation
Amplification
K
R313W
A357V
S487L
FZR1
1
182
WD40
496
L
WT
EV
WT
R313W
A357V
S487L
HA-FZR1
Flag-BRAF
IP: Flag
IB: HA
IB: Flag
IP: HA
IB: Flag
IB: HA
WCL
IB: HA
IB: Flag
M
EV
WT
WT
R313W
A357V
S487L
HA-FZR1
Flag-BRAF
His-UB
Ni-NTA
IB: Flag
WCL
IB: Flag
IB: HA

Figure S6. Pharmacologically inhibiting BRAF/ERK and CDK4 restores the APC^{FZR1} E3 ligase activity.

(A-B) Protein levels of BRAF and other APC^{FZR1} substrates decreased upon $BRAF^{V600E}$ and CDK4/6 inhibition in melanoma cells. IB analysis of WM266.4 $BRAF^{V600D}$ (**A**) and A375 $BRAF^{V600E}$ (**B**) melanoma cells treated with either 1 μM PLX4032 (V600Ei), 10 μM pan-CDK inhibitor mimosine (pan-CDKi), 1 μM CDK4/6 inhibitor PD0332991 (CDK4i), 1 μM PLX4032+10 μM mimosine, 1 μM PLX4032+1 μM PD0332991 or DMSO as a negative control for 24 hours before harvesting.

(C) Depletion of *FZR1* in MEK-inhibited OVCAR8 cells led to the upregulation of BRAF. IB analysis of $BRAF^{WT}$ expressing OVCAR8 cells, which were, infected with the control (shScr) or the indicated sh*FZR1* lentiviral shRNA constructs. The infected cells were selected with 1 μg/ml puromycin for 72 hours to eliminate the non-infected cells before harvesting. Prior to the harvest, cells were treated with DMSO (as a negative control) or 1 μM MEK inhibitor PD0325901 (MEKi) plus 10 μM pan-CDK inhibitor mimosine (CDKi) for 24 hours as indicated.

(D-E) Ubiquitination of APC^{FZR1} substrate Cdc20 was elevated in melanoma cells treated with $BRAF^{V600E}$, MEK and/or CDK4/6 inhibitors. IB analysis of WCL and Ni-NTA (Ni-nitrilotriacetic acid) affinity precipitates derived from $BRAF^{WT}$-expressing HBL (**D**) or $BRAF^{V600E}$-expressing A375 (**E**) cells treated with the indicated inhibitors for 24 hours. Cells were pretreated with 10 μM MG132 for 10 hours before harvesting.

(F-H) FACS analysis to determine cell cycle phase distribution of $BRAF^{V600E}$-expressing A375 (**F**), $BRAF^{V600D}$-expressing WM266.4 (**G**) or $BRAF^{WT}$-expressing HBL (**H**) cells treated with the indicated inhibitors for 24 hours.

(I) Binding between FZR1 and core APC subunits APC8 and APC4 was increased upon ERK and CDK4 inhibition. IB analysis of WCL and anti-FZR1 IP derived from A375 cells treated with the indicated kinase inhibitors. Cells were pretreated with 10 μM MG132 for 10 hours before harvesting.

(J) Distribution of deletions, mutations and copy number amplifications in *FZR1* (*FZR1*) and 9 APC core subunits, as well as in *BRAF*, *NRAS*, *CCND1* (*CYCLIN D1*), *CDK4* and *CDKN2A* genes that are shown across 262 samples from the Skin Cutaneous Melanoma (TCGA, Provisional) dataset (cbioportal.org) (24, 25).

(K) A schematic illustration of the melanoma derived *FZR1* mutations located in the WD40 domain.

(L) Melanoma patient-derived FZR1 mutants failed to bind BRAF. IB analysis of WCL and IP from 293T cells transfected with Flag-BRAF and the indicated HA-FZR1 constructs including melanoma-derived FZR1 mutants. 36 hours post-transfection, cells were pretreated with 10 μM MG132 for 10 hours before harvesting.

(M) Melanoma patient-derived FZR1 mutants failed to promote ubiquitination of BRAF. IB analysis of WCL and Ni-NTA (Ni-nitrilotriacetic acid) affinity precipitates derived from HEK293 cells transfected with Flag-BRAF and the indicated HA-FZR1 constructs. 36 hours post-transfection, cells were pretreated with 10 μM MG132 for 10 hours before harvesting.

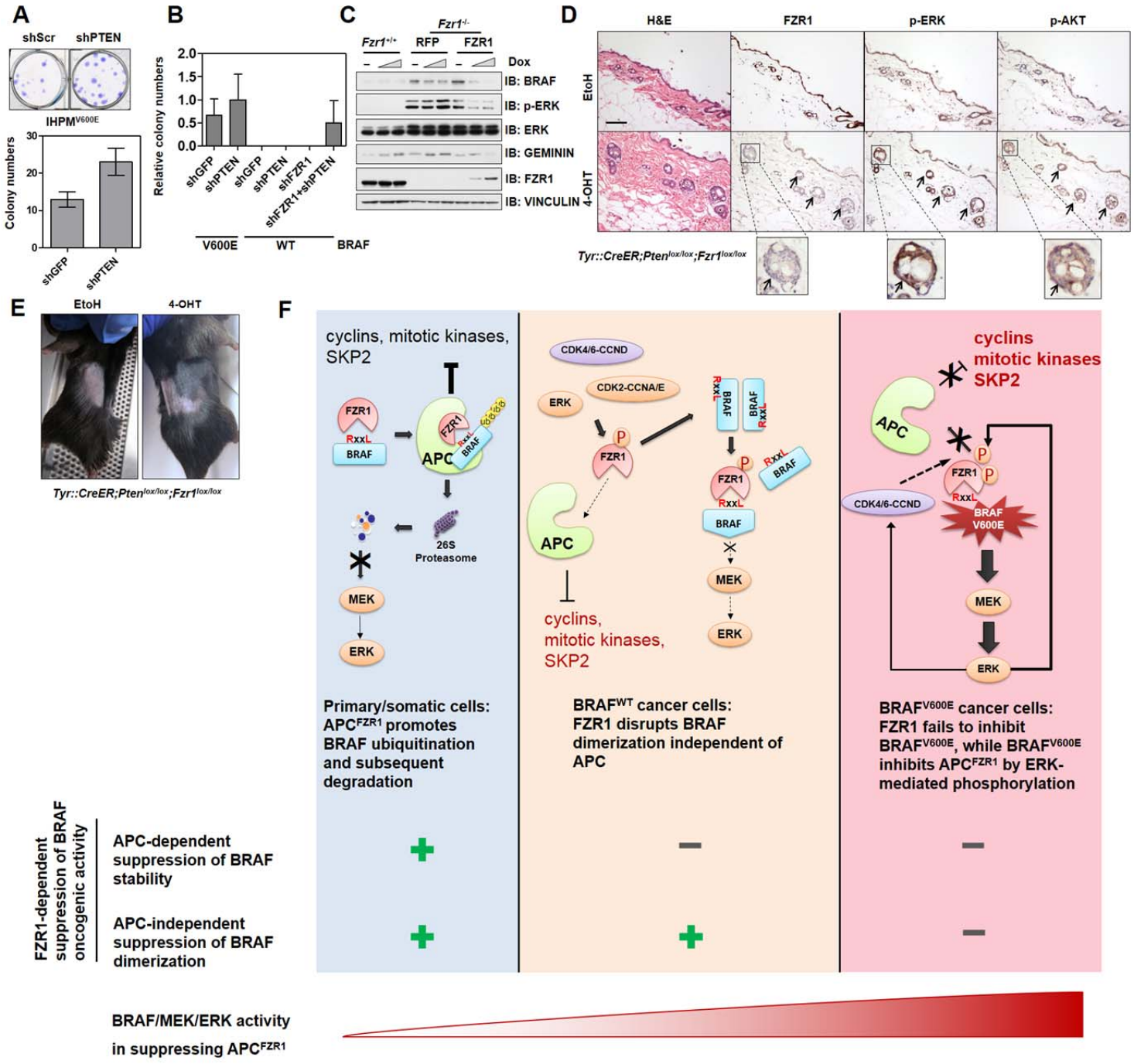
A
shScr
shPTEN
IHPM^V600E
Colony numbers
shGFP
shPTEN
B
Relative colony numbers
shGFP
shPTEN
shGFP
shPTEN
shFZR1
shFZR1+shPTEN
V600E
WT
BRAF
C
Fzr1+/+
Fzr1-/-
RFP
FZR1
Dox
IB: BRAF
IB: p-ERK
IB: ERK
IB: GEMININ
IB: FZR1
IB: VINCULIN
D
H&E
FZR1
p-ERK
p-AKT
EtoH
4-OHT
Tyr::CreER;Pten^lox/lox;Fzr1^lox/lox
E
EtoH
4-OHT
Tyr::CreER;Pten^lox/lox;Fzr1^lox/lox
F
cyclins, mitotic kinases, SKP2
FZR1
RxxL
BRAF
APC
26S Proteasome
MEK
ERK
Primary/somatic cells: APC^FZR1 promotes BRAF ubiquitination and subsequent degradation
CDK4/6-CCND
CDK2-CCNA/E
ERK
P
FZR1
APC
cyclins, mitotic kinases, SKP2
BRAF
RxxL
MEK
ERK
BRAF^WT cancer cells: FZR1 disrupts BRAF dimerization independent of APC
cyclins mitotic kinases SKP2
APC
FZR1
CDK4/6-CCND
BRAF V600E
MEK
ERK
BRAF^V600E cancer cells: FZR1 fails to inhibit BRAF^V600E, while BRAF^V600E inhibits APC^FZR1 by ERK-mediated phosphorylation
FZR1-dependent suppression of BRAF oncogenic activity
APC-dependent suppression of BRAF stability
APC-independent suppression of BRAF dimerization
BRAF/MEK/ERK activity in suppressing APC^FZR1

Figure S7. Depletion of *FZR1* co-operates with *PTEN* deficiency to promote co-activation of BRAF/ERK and AKT oncogenic signaling both *in vitro* and *in vivo*.

(A) Depletion of *PTEN* augmented proliferation of IHPM^{V600E} cells. IHPM^{V600E} cells generated in **Fig. 7A** were subjected to clonogenic survival assays in RPMI-1640 media supplemented with 10% FBS without the essential growth factor, TPA for 21 days. Crystal violet was used to stain the formed colonies and the colony numbers were counted from three independent experiments. The colony numbers were calculated as mean ± SD**.**

(B) Anchorage- and TPA-independent growth of IHPM cells in soft agar upon co-depletion of *FZR1* and *PTEN*. IHPM cells generated in **Fig. 7A** were seeded (30,000 cells per well) in 0.5% low-melting-point agarose in RPMI-1640 with 10% FBS, layered onto 0.8% agarose in RPMI-1640 with 10% FBS without TPA. The plates were cultured for 80 days whereupon the colonies >50 μm were counted under a light microscope. The colony numbers were plotted as mean ± SD from three independent experiments.

(C) Doxycycline-induced expression of FZR1 led to the decrease of BRAF protein abundance and ERK activity in *Fzr1*$^{-/-}$ MEFs. *Fzr1*$^{-/-}$ MEFs were infected with pTRIPZ lentiviral vectors that allow the ectopic expression of either RFP (as a negative control) or *FZR1* cDNA under the control of doxycycline. The infected cells were selected with 1 μg/ml puromycin for 72 hours to eliminate non-infected cells. Afterwards, 300 ng/mL doxycycline were added for 24 hour before harvesting.

(D) Elevation of both p-AKT and p-ERK was found in mouse skin samples derived from melanocyte conditional *FZR1* knockout mice. H&E as well as immunohistochemistry analysis of flank skin tissues derived from **Fig. 7E** using anti-p-AKT, anti-p-ERK and anti-FZR1 antibodies as indicated. Arrows indicate the positively stained cells around hair follicles that are putative melanocytes. Scale bar: 100 μm.

(E) A representative picture of *Tyr::CreER;Pten*$^{lox/lox}$*;Fzr1*$^{lox/lox}$ mice that developed pigmented lesions 3 weeks after topical administration of 4-OHT.

(F) A schematic illustration of proposed models for the putative roles of FZR1 in suppressing the BRAF oncogenic signaling via different mechanisms in different cellular contexts and tumor developmental stages.

	TCGA (total 287 cases)	*Broad (total 121 cases)*	*Yale (total 91 cases)*
FZR1 and 14 APC subunits	21.8% mutation or deletion	19.8% mutation	14.3% mutation
FZR1	3.5% mutation or deletion	No mutation or deletion found	4.4% mutation
APC1	5.7%	5%	2.2%
APC2	2.7%	1.7%	2.2%
CDC27	5.3%	4.1%	2.2%
APC4	3.4%	4.1%	4.4%
APC5	4.6%	1.7%	No mutation or deletion found
CDC16	2.3%	1.7%	1.1%
APC7	2.3%	No mutation or deletion found	1.1%
CDC23	1.1%	0.8%	1.1%
APC10	1.9%	No mutation or deletion found	No mutation or deletion found
APC11	4.6%	No mutation or deletion found	No mutation or deletion found
CDC26	No mutation or deletion found	0.8%	No mutation or deletion found
APC13	No mutation or deletion found	No mutation or deletion found	No mutation or deletion found
APC15	3.8%	No mutation or deletion found	No mutation or deletion found
APC16	0.8%	No mutation or deletion found	0.8%

Supplementary Table S1. Mutation and deletion of *FZR1* and 14 APC core complex subunits identified in melanoma patients from the TCGA melanoma dataset (cbioportal.org).